Earth Syst. Dynam. Discuss., 5, 809–848, 2014
www.earth-syst-dynam-discuss.net/5/809/2014/
doi:10.5194/esdd-5-809-2014

Earth System Dynamics Discussions
Open Access

Temporal variations in atmospheric CO_2 on Rishiri Island in 2006–2013: responses of the interannual variation in amplitude to climate and the terrestrial sink in East Asia

C. Zhu[1,*] and H. Yoshikawa-Inoue[2]

[1]Graduate School of Environmental Science, Hokkaido University, Sapporo, 060-0810, Japan
[2]Faculty of Environmental Earth Science, Hokkaido University, Sapporo, 060-0810, Japan
[*]now at: Institute of Low Temperature Science, Hokkaido University, Sapporo, 060-0819, Japan

Received: 30 May 2014 – Accepted: 19 June 2014 – Published: 27 June 2014

Correspondence to: C. Zhu (chmzhu@pop.lowtem.hokudai.ac.jp)

Published by Copernicus Publications on behalf of the European Geosciences Union.

Abstract

Surface observation of the atmospheric CO_2 mixing ratio implies the combined influences of both natural fluctuations and anthropogenic activities on the carbon cycle. Atmospheric CO_2 has been measured on Rishiri Island in the outflow region of Eurasia since May 2006. We report the first 7 year temporal atmospheric CO_2 variations from diurnal to interannual scales. In the diurnal scale, an obvious cycle appeared as a minimum in the afternoon and maximum at midnight in the summer months. Seasonally, the maximum CO_2 concentration appeared around the beginning of April, while the minimum appeared around the middle of August. A mean growing season length of ~ 126 days was estimated. In the period from 2007 to 2012, the peak-to-peak amplitude increased until 2009 and decreased thereafter, with a mean value of 19.7 ppm. In the long term, atmospheric CO_2 is increasing by a mean growth rate of 2.1 ppm year^{-1}. Investigations on the driving climatic factors on the interannual variation in amplitude indicated that temperature in East Asia (40–60° N, 90–150° E) affected the CO_2 amplitude by affecting the seasonal maximum, with a time lag of 1–2 years. On the contrary, precipitation did not likely affect CO_2 amplitudes. The amplitude also responded to a natural carbon source/sink variation in East Asia. We suggest that temperature in the first year would affect carbon sinks in the second year in the fetch regions, which further affect CO_2 amplitude mainly through ecosystem respiration. Circulation changes also likely contributed to the decreasing amplitude since 2009, as indicated by the simultaneous decrease in the ^{222}Rn concentration in spring and summer.

1 Introduction

Atmospheric carbon dioxide (CO_2) is a major contributor (1.82 out of a total of 2.83 W m^{-2} in 2011) to radiative forcing, a measure that determines the effect of greenhouse gases on the climate (Myhre et al., 2013). From 1990 to 2012, total radiative forcing increased by 32 %, of which CO_2 accounted for ~ 80 % (NOAA–ESRL, 2014). In the

ESDD
5, 809–848, 2014

viewpoint of the biogeochemical cycle, three processes dominate the turnover of atmospheric CO_2. They are the exchange of atmospheric CO_2 with the terrestrial biosphere, the exchange of atmospheric CO_2 with the ocean, and the one-dimensional emission of CO_2 to the atmosphere from anthropogenic activities. Globally, there are exchanges between the atmosphere and the terrestrial biosphere of approximately 110 gigatonnes (Gt) carbon per year. The exchange with the ocean is approximately 80 Gt year^{-1} (Ciais et al., 2013). In addition, anthropogenic activities that are primarily caused by fossil fuel use, cement production and land use change emit approximately 9 Gt C year^{-1} (DOE US, 2008). Of these, around half are absorbed by the terrestrial biosphere and the ocean, while the other half remain in the atmosphere. This anthropogenic emission of CO_2 is believed to be the dominant cause of global warming.

A group of studies have been conducted to understand the carbon cycle. The approaches that have been adopted are generally in the two categories known as bottom-up and top-down. In the bottom-up approaches, CO_2 fluxes are estimated from the land, ocean and human activities (e.g. Keeling et al., 2011; Prytherch et al., 2010; Saigusa et al., 2008). However, misreporting occurs as a result of simple error, ignorance, or intention (Nisbet and Weiss, 2010). This makes top-down verification significant because it is based on observations. The top-down approaches are a type of direct estimation, after all sources and sinks are contained in the resulting CO_2 mixing ratio (concentration). This is a valuable tool to validate carbon inventories estimated by the bottom-up approach (e.g. Carouge et al., 2010a, b). It also constitutes the basic information for building models (Rödenbeck et al., 2009). Measurements of atmospheric CO_2 thus turn out to be the basis for top-down flux estimations.

The first continuous in situ measurements of atmospheric CO_2 started in 1958 at Mauna Loa (MLO), in parallel with the flask sampling in the South Pole in 1957 (Keeling, 1960; Keeling et al., 1989). The observational network was thereafter expanded, covering most regions from the arctic to the South Pole (Komhyr et al., 1985; WMO, 1992). Currently, the network provides global coverage from remote islands to highly populated regions, by surface sites (e.g. Peters et al., 2010; Wunch et al., 2013), aircraft

ESDD
5, 809–848, 2014

(e.g. Niwa et al., 2011, 2012, 2014; Patra et al., 2011), and satellites (Maksyutov et al., 2013; Wunch et al., 2013). The observed data document both the natural oscillation of the global environment and the changing climate resulting from anthropogenic activities. In the Northern Hemisphere, there is consensus that the seasonal variation in atmospheric CO_2 is caused by the changes in photosynthesis and respiration of the terrestrial ecosystem. This is likely induced by temperature and precipitation changes (e.g. Buermann et al., 2007; Keeling et al., 1996). On the other hand, the long-term increasing trend was mainly due to anthropogenic emission and land use changes (Francey et al., 2010; Thoning et al., 1989).

In East Asia, it was reported that anthropogenic CO_2 emissions and other pollutants have been increasing in the past decades (e.g. Akimoto, 2003; Fang et al., 2014). Meanwhile, boreal forests in the middle to eastern part of the Eurasian continent contribute critically to atmospheric CO_2 variations and global carbon budgets (Ciais et al., 2010; Peylin et al., 2013; Piao et al., 2011). For the 1.42 billion hectares of boreal forests in the world, the biomass sink was estimated to be 0.68 ± 0.34 billion tons C year^{-1}, of which nearly 70 % was in Eurasia (Myneni et al., 2001). Consequently, the sources and sinks from both natural and anthropogenic sectors would influence surface CO_2 levels in East Asia.

There are CO_2 observation stations in the remote islands of the open oceans, such as the Mauna Loa Observatory (Fig. 1). The remote sites have the advantage of representing the continental scale of reference levels of trace gases. For example, the observed CO_2 variation at the MLO site is co-influenced by both the Eurasian and the North American continents (Buermann et al., 2007; Lintner et al., 2006). On the other hand, there are inland sites that are more convenient for catching synoptic pollution events (e.g. Levin et al., 1995; Ramonet et al., 2010; Zhou et al., 2003). In the boundary between the continent and the ocean, observation sites are expected to catch regional phenomena from synoptic to long-term scales. Along the western Pacific Rim, a few sites in East Asia were established in the observation network (WMO, 2013). For example, based on observations of atmospheric CO_2 and O_2 concentrations at Hateruma,

ESDD
5, 809–848, 2014

Minejima et al. (2012) constrained the compositions of fossil fuel types in China, Korea and Japan based on changes in the $\Delta O_2/\Delta CO_2$ molar ratio during pollution events.

Rishiri Island is the northernmost site in Japan where atmospheric greenhouse gases are measured, although it is not yet being incorporated by the WMO. Previous studies indicated that it is co-influenced by continental and maritime fetches, when the continental fetches are mainly in 90–150° E, 40–60° N (Zhu et al., 2012). This region includes part of the extensive boreal forests from the middle to eastern Eurasian Continent (Lefsky, 2010). The changes in carbon sources and sinks in this region contribute critically to the variation in atmospheric CO_2 and global carbon budgets. Since May 2006, atmospheric CO_2 has been continuously measured at Rishiri (Inoue et al., 2008). In this work, we report the first 7 years of atmospheric CO_2 data showing the temporal variations from the diurnal to interannual scales. Our purposes are (1) to examine the seasonal cycle and the inferred regional phenology; (2) to investigate the interannual amplitude variation (IAV); and (3) to investigate the environmental and circulation-related factors controlling the IAV.

2 Experimental section

2.1 The Rishiri Observatory

Rishiri is the northernmost island of Japan, with 5500 residents and an area of 182 km^2. Its natural attributes are well protected in the territory of the Rishiri-Rebun-Sarobetsu National Park with no industry (Fig. 1). The center of the island is occupied by Mt. Rishiri (1721 m), which is a Quaternary stratovolcano. Rishiri Observatory (RIO) is located at the south foot of Mt. Rishiri, at approximately 35 m a.s.l. It faces south-southwest at a distance of ~ 800 m from the coast. The temperature of the laboratory has been controlled at ~ 20 °C.

ESDD
5, 809–848, 2014

2.2 Atmospheric CO_2 measurement

During sampling, ambient air was drawn at 10 L min^{-1} by a diaphragm pump from ~ 4 m above the ground through a 0.25 in Teflon tube. In the laboratory, an aliquot of air (0.2 L min^{-1}) was passed through an electric dehumidifier and Nafion tube (Perma Pure, Inc., USA) to remove water vapor. A heatless dryer (CKD HD-0.5, CKD Co., Ltd.) was used to supply the Nafion tube dry air. After removal of water vapor, the air sample was introduced into the sample cell of a non-dispersive infrared gas (NDIR) analyzer (LI 6262, LI-COR Inc., USA) for 4 min, and the airflow was stopped to establish temperature and pressure equilibrium. Twenty-five seconds later, the output voltage of the NDIR analyzer was integrated for 30 s by a programmable logic controller (Yokogawa FA-M3R). The CO_2 concentration was obtained every 5 min and averaged over 1 h.

The NDIR analyzer was calibrated every 4 h (8 h during nighttime) by successively introducing four calibrated working gases (340, 380, 420, and 450 ppm CO_2 in dry air) into the NDIR analyzer cell for 5 min each. The CO_2 concentrations of the working gases are traceable to the WMO mole fraction scale (Inoue and Matsueda, 2001). The drift of the output voltage of the NDIR analyzer was estimated by a linear interpolation of two successive sets of calibration data. Based on the replicated measurements of a sample gas in the cylinder, the precision of analysis ($\pm 1\sigma$) was estimated to be smaller than 0.1 ppm during daytime and equal to or slightly larger than 0.1 ppm during nighttime (21:00–05:00 local time, LT).

2.3 Extracting the seasonal cycle and the long-term trend

The observed atmospheric CO_2 records consist of three components (e.g. Keeling et al., 1996). The first is the local contribution, which leads to the short time variation on a time scale of several hours. The second is the seasonal cycle within a period of one year. This is caused by the "breathing" of the land biosphere, which includes the summer photosynthesis and winter respiration. The third one is the long-term increasing trend, which is believed to be caused by the anthropogenic activities after

ESDD
5, 809–848, 2014

the industrial revolution as a result of fossil fuel consumption and land use change. To investigate the seasonal and long-term trends of atmospheric CO_2, the data were selected to reflect regional- to global-scale variations and were subjected to a curve-fitting method. Details on the selection and curve fitting are described in the Supplement, and a brief description will be given is this section.

Hourly data were first selected to remove local influences. We examined the data continuity after selecting data using thresholds (0.25, 0.5 and 1 ppm) for hour-to-hour variations (any or both consecutive hours) (Fig. S1 in the Supplement). We finally kept those hours if the variations between any two consecutive hourly values were less than 0.25 ppm, a method that was also used by Thoning et al. (1989) for the analysis of Mauna Loa data. After this selection, 47.4 % of the original record was retained. We then examined the daily means using different hours of the day (daytime, nighttime and transition hours) to minimize local influences. Daily means calculated from daytime hours (10:00–15:00 LT) had the lowest noise level and apparent baseline and were chosen to examine large-scale variations (Fig. S2 in the Supplement). This dataset for curve fitting used 14.1 % of the original record.

For the calculated daily means, a curve-fitting method including function fit and residuals filtering was applied to extract seasonal cycles and secular trends following Thoning et al. (1989). Both the numbers of polynomial terms and harmonics of the function fit were set as 3 (Fig. S3a). During the residuals filtering, the cutoff frequencies for the short- and long-term variations were set at 120 and 667 d, respectively (Fig. S3b).

2.4 Ancillary data

The IAV at RIO was compared with that of MLO and Shemya Island (SHM, 52.72° N, 174.10° E). CO_2 data at these sites were obtained from NOAA (Tans and Keeling, 2014). The climatic factors controlling the IAV in association with the fetch region previously reported were analyzed (Zhu et al., 2012). Monthly land temperature and precipitation anomaly data with $5^\circ \times 5^\circ$ resolution were obtained from the United States

ESDD
5, 809–848, 2014

National Climate Data Center (Jones and Moberg, 2003; Peterson and Russell, 1997). The temperature anomaly was evaluated for the period 1981–2000, while the precipitation anomaly was evaluated for 1961–1990. The monthly land temperature and precipitation anomalies over East Asia (EA, 40–60° N, 90–150° E), broader East Asia (BEA, 15–75° N, 90–180° E), the Northern Hemisphere (NH) and the globe (GL) were calculated over 2004–2013. The linear relationships between these climatic parameters and the IAV were investigated. The relationship between IAV with carbon sink strengths (Net Ecosystem Production, NEP) in EA and BEA was also investigated to elucidate the underlying mechanisms. The NEP data were obtained from CarbonTracker Europe as gridded flux (Peters et al., 2007, 2010). The possible changes in circulation around RIO that contribute to IAV derived from atmospheric ^{222}Rn were investigated. Measurement of atmospheric ^{222}Rn at RIO was described elsewhere (Zhu et al., 2012).

The growth rate was examined with respect to the influences of fossil fuel emissions on regional and global scales and natural oscillations in terms of the El Niño/Southern Oscillation (ENSO) and the North Pacific Index (NPI). The fossil fuel emission data were obtained from the Carbon Dioxide Information Analysis Center (CDIAC) (Boden et al., 2013). The ENSO index data were obtained from NOAA (http://www.cpc.ncep.noaa.gov/data/indices/soi). The NPI data were obtained from The National Center for Atmospheric Research (NCAR) (Hurrell et al., 2013).

The planetary boundary layer height and local wind direction were used to discuss local meteorology on diurnal CO_2 variations. Planetary boundary layer height was extracted from the Climate Forecast System Reanalysis of the University Corporation for Atmospheric Research (UCAR) Data Archives (Saha et al., 2010). Wind direction was measured at Kutsukata meteorological station, which is approximately 11 km from RIO, where the data were obtained from the Japan Meteorological Agency (http://www.jma.go.jp).

ESDD
5, 809–848, 2014

3 CO_2 variation from diurnal to interannual scales

3.1 Data overview

Among all 66 504 h from May 2006 to November 2013, there are 5637 h in which CO_2 was not recorded because of system maintenance, power blackouts, and so on. In other words, 91.5 % of the hours were recorded. Atmospheric CO_2 at Rishiri Island indicated clear seasonal cycles caused by the seasonal change in photosynthetic strengths, as observed at other typical mid-latitude sites in the Northern Hemisphere (Fig. 2). In addition, large episodic high CO_2 events appeared frequently and exclusively during the summer months. This is likely to be caused by (1) the high emissions from the local soil and vegetation, and (2) the formation of a stable nocturnal boundary layer, as is discussed in the next section.

3.2 Diurnal variation

Figure 3 shows the diurnal variation of atmospheric CO_2 at Rishiri Island obtained from the 7 year records. To obtain the anomalies in Fig. 3, the mean CO_2 concentration at each hour of the month was first calculated. The anomalies were then calculated as the departure of each hourly value from the 24 h means of the month. In the different months of a year, the diurnal CO_2 cycle varied greatly. From May to October, a prominent diurnal variation appeared in the amplitudes ranging from 8.1 to 31.0 ppm (Fig. S4 in the Supplement), while the largest values were in July–August (29.5–31.0 ppm). In these summer months, the CO_2 concentration decreased rapidly for 2–3 h in the early morning after sunrise. From around 08:00 LT, CO_2 tended to be relatively steady at low concentrations during the daytime until around 16:00 LT. From sunset to the early evening, CO_2 concentration increased rapidly for another 2–3 h. During the nighttime from ~ 20:00 to ~ 04:00 LT, CO_2 concentrations were relatively steady at high concentrations. On the contrary, from November to April, the amplitudes of the diurnal variation were within the relatively small range of 0.7–3.3 ppm. The lowest diurnal amplitude

ESDD
5, 809–848, 2014

(0.7 ppm) appeared in December–February in which the diurnal cycle with nighttime high and daytime low concentrations was still obvious.

Several factors contribute to this phenomenon in the summer months. The first factor is that of the diurnal variation of the height of the mixing layer. Nocturnal stable boundary layers were formed that broke up in the daytime during calm days (Fig. S5a in the Supplement). This phenomenon also caused the diurnal variation of ^{222}Rn in the summer (Zhu et al., 2012). The second factor is the local vegetation. Local plants caused a photosynthetic drawdown during the daytime, when the respiration by plants and soil contributed to the nighttime buildup. However, in regions where photosynthesis dominates daytime drawdown, CO_2 frequently decreased continuously until reaching an afternoon minimum (Haszpra et al., 2008; Murayama et al., 2003; Thoning et al., 1989). We therefore explored the meteorological drivers in terms of local topography.

The observatory is located on the seashore on the southern foot of Mt. Rishiri, where both the sea–land breeze and the mountain–valley airflow would exert an influence on the atmospheric observations. Local meteorology indicates that there is an onshore wind during daytime and offshore winds during the night. For example, during 6–13 June 2011, a diurnal wind pattern appeared when the wind came mainly from the north where Mt. Rishiri is located, while during the daytime, it comes from the ocean (west, east and south) (Fig. S5b in the Supplement). Continuous fresh air coming in from the surface of the ocean during daytime is likely causing the flat CO_2 pattern in the afternoon.

On the other hand, in sites with flat terrain, the nighttime CO_2 buildup indicated a continuously increasing pattern, such as at Hegyhátsál, Hungary (Haszpra et al., 2008). However, at sites adjacent to the mountains, the nighttime buildup had a flat pattern, as was observed at Takayama, Japan (Murayama et al., 2003). This was related to the drainage wind from the top of the mountain that brings air from the free atmosphere with low CO_2. The present result of a flat nighttime buildup pattern indicated that the CO_2 from nighttime respiration in summer is diluted. There were some high-concentration episodic events that appeared in the nighttime hours (Figs. 2 and

ESDD
5, 809–848, 2014

S4b in the Supplement). During these hours, the weather was often calm with a near-zero wind speed. For example, in 2011, the mean wind speed was 1.2 m s^{-1} during those hours (a total of 259 h) when the observed CO_2 concentrations were higher than 420 ppm, and it was 0.9 m s^{-1} in the hours (a total of 70 h) when the CO_2 concentrations were higher than 450 ppm. These hours are removed to eliminate local influences.

3.3 The seasonal cycle

3.3.1 Seasonal amplitude

The calculated smoothed fit and the long-term trend along with the daily means were plotted in Fig. 4a. The de-trended seasonal cycle (ΔCO_2) and the growth rate were plotted in Fig. 4b. The maxima, minima and yearly peak-to-peak amplitudes were obtained from ΔCO_2. The mean seasonal amplitude of 19.7 ± 1.6 ppm was estimated with a maximum ΔCO_2 of 7.1 ± 0.4 ppm and a minimum of −12.5 ± 1.2 ppm (Fig. 5a). Interannually, the seasonal amplitude increased until 2009 and decreased thereafter. The variation was similar to that at SHM, located in the western North Pacific (Figs. 1 and 5b). However, the magnitude at RIO was slightly larger than that at SHM in 2007–2010. This was because RIO was closer to the Eurasian continent and tending to be more sensitive to terrestrial sources/sinks. The magnitude of ΔCO_2 at RIO was much larger than at MLO (Figs. 1 and 5b), indicating the increased effect of the terrestrial biosphere in the Eurasian continent on the ambient level at RIO. The magnitude difference was also related to the latitudinal gradient because there was an amplitude decrease toward the south in the Northern Hemisphere (Conway et al., 1994; Keeling et al., 1996). The altitude difference between RIO (35 m) and MLO (3397 m) might be another reason. The factors that possibly affected the IAV were the variation in the carbon source and sink strength (e.g. Graven et al., 2013) and the changes in air circulation. These constraints will be discussed in Sect. 4.

ESDD
5, 809–848, 2014

3.3.2 The variation phase

The day of the year on which the maximum CO_2 concentrations appear marked the changing of the phenology of the terrestrial biosphere from the dormant season to the growing season. Similarly, the day of minimum CO_2 concentration was an index of the shift from the growing to the dormant season (Piao et al., 2007; Richardson et al., 2010). At RIO, the maximum CO_2 appeared on 3 April (Day of Year, DOY 93) ±5.3 d, and the minimum appeared on 8 August (DOY 220) ±5.0 d (Fig. 6a). As the smoothed curve around the maximum and minimum days varied quite smoothly, comparatively large interannual variations of the date appeared. Similar indices showing the phase of the seasonal cycle were the days when the fitted seasonal cycle crosses the long-term trend. These were the days when the drawdown of the seasonal cycle crosses the long-term trend (the zero-crossing day) and the buildup of the seasonal cycle cross the long-term trend (the buildup day). The zero-crossing day appeared on 2 June (DOY 153) ±3.9 d, and the buildup day appeared on 23 October (DOY 296) ±3.6 d (Fig. 6b).

Based on the Normalized Difference Vegetation Index (NDVI) and analysis of the climatic parameters of the spring phenology in six temperate biomes of China for the period of 1982–2006, Wu et al. (2012) found that the spring phenology in most areas showed obvious advancing trends during the 1980s and early 1990s and delaying trends thereafter. For this 7 year observation period, the present result of both the maximum and minimum days, and the zero-crossing and the buildup days did not show an evident shifting trend in phenology.

In the period of CO_2 drawdown between the maximum and minimum days, the photosynthetic absorption by the terrestrial biosphere was much greater than the respiration. This period could therefore serve as an index of the growing season length. This length was estimated at 126.3 ± 6.7 d (Fig. 7). The longest growing season was observed in 2010 by 135 days, while the shortest periods appeared in 2008 and 2013 by 120 and 116 days, respectively. From 2008 to 2010, the growing season increased by 15 days. Thereafter, it decreased until 2013 by 19 days.

ESDD
5, 809–848, 2014

The period between the zero-crossing and buildup days could also be assumed as the summer half of the year. Based on the observed CO_2 variation, the length of the summer half was estimated at 143.1 ± 6.7 d (Fig. 7). The longest summer half appeared in 2012 at 153 days, while the shortest summer half year of observation period was in 2008 at 134 days. Recent studies suggested the extension of the length of the growing season both in East Asia and around the world in recent decades (Chen et al., 2005; Cong et al., 2012; Jeong et al., 2011). Longer-term observations are needed to examine the relations between the vegetation growing phase and the CO_2 variation phase changes.

4 The controlling factors on IAV

4.1 The effect of temperature and precipitation on IAV

Previous studies indicated that the dominant continental fetch regions that affect RIO were in the range of 40–60° N, 90–150° E of East Asia (Zhu et al., 2012). A recent simulation using the transport model NICAM-TM on the footprint of RIO produced similar results (Y. Niwa, personal communication, 2014). Although RIO was also influenced by the maritime fetch regions, especially in summer, they brought about an air mass with a background or quasi-background level of CO_2. The variations of the air–sea CO_2 flux in comparison with the air–land flux are quite small (Lee et al., 1998; Séférian et al., 2013). Given this fact, the interannual CO_2 variations at RIO are likely dominantly affected by the sources and sinks in the fetch regions of the Eurasian continent. The effects of temperature and precipitation from regional to global scales on the observed IAV were examined.

In the climate–vegetation–CO_2 relations, the climatic variations caused the changes in terrestrial carbon fluxes, leading to the variations of atmospheric CO_2 level (e.g. Yu et al., 2012). Therefore, CO_2 amplitude in the current year, determined by the maximum and minimum ΔCO_2, is determined by the climate and the sink strength during the

ESDD
5, 809–848, 2014

previous months. To constrain this, the relations between amplitude and temperature and precipitation anomalies in different periods of previous months in EA, BEA, NH and GL were investigated (Table S1 in the Supplement). On an annual scale, the amplitude anomaly was not related to temperature anomalies on any spatial scale in the current year. It was also not constrained by temperature anomalies during the months of the previous year. However, the amplitude anomaly at Rishiri was significantly affected by temperature anomalies in the period from April of 2 years before until the previous March, in EA and BEA (with 1 year time-lag, $p < 0.01$, Fig. 8a and b). Certain shorter time periods within this longer period, specifically August–March, October–March and March itself, are influenced to different degrees ($p < 0.05$, Table 1). On the other hand, there were no impacts of precipitation anomalies on amplitude without or with time lags (Tables S1 in the Supplement and 1). The effect of temperature on the components of the amplitude was investigated further. In association with the phase variation (the CO_2 drawdown and buildup days), this investigation was performed by examining the effect of the lagged temperature anomalies in different periods on the maximum and minimum ΔCO_2 values. With a 1 year time-lag (mean temperature anomalies over previous 1–2 years), temperatures strongly affected the maximum ΔCO_2 and to some degree affected the minimum ΔCO_2 (Table 2).

A similar phenomenon was also observed at MLO where the East Eurasia temperature at mid-to-high latitudes caused a 1–2 year lagged amplitude (Buermann et al., 2007). Several possible mechanisms underlie this phenomenon. The first is the lagged response of the terrestrial biosphere to temperature. Braswell et al. (1997) reported that there was a 1–2 year lagged response of NDVI to temperature anomalies, especially in the boreal ecosystems. Their results indicated that the source and sink strengths of the terrestrial biosphere for the current season are associated with the climatic variability in the previous several years. Similarly, Zeng et al. (2008) predicted the vegetation dynamics using climate variables with lead times up to 9 months. In North America, Zhang et al. (2013) reported that an intensified net carbon uptake during the eastern boreal growing season in North America was led by increased precipitation anomalies

ESDD
5, 809–848, 2014

in the previous year and attributed this lagged influence to "climate memory" carried by regional snowmelt water. However, in the western boreal North America, the carbon response lags behind the temperature anomalies by approximately 6 months. The controlling climatic variables on terrestrial carbon balance no doubt varied in different places, probably as a result of vegetation changes. The second possible reason is the turnover time of plant leaf litter, wood and other fine organic matter. Although a direct response to the climate was frequently observed, reconciliation of the carbon budget of a mid-latitude forest covered several years (Barford et al., 2001). This also indicated that the climatic influences on vegetation and therefore on the CO_2 level have a longer time scale. Finally, other than the direct effects on photosynthesis and respiration, climatic parameters would cause the indirect effects on the biological and ecological processes dominating the carbon flux. Hui et al. (2003) termed this effect as "functional change". These functional change effects had been reported in bog and prairie ecosystems (Wayne Polley et al., 2008; Teklemariam et al., 2010).

Our estimation of better relations between the leading temperature anomalies and the maximum ΔCO_2 implied that the soil respiration is playing a more important role in affecting CO_2 amplitude. This is because soil respiration is the main contribution to ecosystem respiration (Re) and is mostly regulated by the air and soil temperature (e.g. Bond-Lamberty and Thomson, 2010; Janssens et al., 2002; Mahecha et al., 2010), especially in the dormant season (e.g. Monson et al., 2006; Zhu et al., 2014). A recent study revealed that global SOC (soil organic carbon) stock changes could be well explained by a temperature anomaly with a resolution of 1–2 °C, while the effect of the precipitation anomaly was negligible (Nishina et al., 2014).

IAV was further examined for its relation with carbon source/sink strengths. It was found that amplitude anomalies were significantly related with NEP anomalies in the previous year in EA (Fig. 8c), where the dominant vegetation is boreal forest. Meanwhile, NEP anomalies positively responded to temperature anomalies (Fig. S6 in the Supplement). Considering together the 1–2 yearly lagged responses of IAV to temperature, we suggest that temperature (first year) impacts the ecosystem carbon sink

ESDD
5, 809–848, 2014

in the next year (second year), where warming would cause an intensified sink. The resulting higher sequestration would further cause a larger CO_2 amplitude in the following year (third year) through an enlarged Re, especially in the dormant season. In future work, it will be crucial to unveil the mechanisms of these lagged responses of the CO_2 level/ecosystem function to the climatic variables to understand the interactions among the climate, the biosphere and the atmosphere.

4.2 Circulation changes

Changes in source regions affect atmospheric compositions at receptors (Fleming et al., 2012). Thus, possible interannual changes in circulation would influence the variations of amplitude. Previous studies have proven the effect of circulation changes on the observed CO_2 seasonal cycle (Higuchi et al., 2002; Murayama et al., 2007).

At RIO, it was found that the ^{222}Rn concentration has decreased interannually since 2009 (Fig. S7 in the Supplement). Investigations on interannual variations in different seasons indicated that the decrease was statistically significant in spring by a rate of $-0.11\,Bq\,m^{-3}\,year^{-1}$ ($R^2 = 0.84$, $p < 0.05$). This implied a change in circulation with decreasing continental fetch and increasing maritime fetch so long as source strengths remain constant. Further investigation indicated that there were positive relations between the maximum ΔCO_2 and ^{222}Rn in the spring and between the absolute value of minimum ΔCO_2 and ^{222}Rn in summer (Fig. 9). Although these relations did not reached the statistically significant level with the short period of 5 years of data, the results implied that the decreasing amplitudes at RIO were also likely caused by the change in air circulation. Kimoto (2005) predicted an increased activity of the East Asia monsoonal rain band in summer associated with the strengthening of anti-cyclonic cells to its south and north. This might bring about an increased influence of the summer maritime fetches to RIO. Meanwhile, Patra et al. (2005) reported that interannual variability of the inversed estimated CO_2 flux in boreal Asia was closely linked with the Arctic Oscillation. The relationship between interannual changes in circulation and atmospheric

ESDD
5, 809–848, 2014

CO_2 amplitude at RIO might be related to the change in ecosystem that was discussed in Sect. 4.1.

5 The growth rate

Other than the seasonal cycle, another part of the signal is the long-term trend. The long-term trend is frequently discussed in terms of variations in growth rate (e.g. Thoning et al., 1989; Wang et al., 2014). The annual CO_2 growth rate at RIO was in the range of 1.7–3.4 ppm year^{-1} from 2007 to 2012, with an average of 2.1 ppm year^{-1} during this period (Fig. 10). The magnitude as well as the trend were similar to that at MLO.

The long-term CO_2 trend was frequently related to large-scale phenomena, such as ENSO. The linear regression of the monthly CO_2 growth rate at RIO with an ENSO proxy against the Southern Oscillation Index (SOI) was examined. The results indicated that there was a lagged negative response of the growth rate to SOI. Specifically, the maximum SOI occurred 8 months before the minimum growth rate (Fig. 11a). This was longer than such a relation for MLO, where a 6 month lagged negative response of growth rate to SOI was observed (Thoning et al., 1989). As the uniform atmospheric mixing in the Northern Hemisphere occurs within 2–3 months (Czeplak and Junge, 1974), this "teleconnection" is explained based on the air circulation.

NPI is another index defined to measure interannual to decadal variations in the atmospheric circulation, which is calculated as the area-weighted sea level pressure over the region 30–65° N, 160° E–140° W (Hurrell et al., 2013). We estimated a lagged negative response of growth rate to NPI, where the maximum NPI occurred ~ 3 months before the minimum growth rate (Fig. 11b). These results suggested that the circulation changes would cause growth rate variations. However, as the investigations of the long-term trend (growth rate) often require a long period record (Francey et al., 2010; Ito, 2011), the controlling factors on the growth rate at RIO should be studied in the future in comparison with other sites.

ESDD
5, 809–848, 2014

6 Conclusions

The seven-year time series CO_2 data at Rishiri Island were analyzed to constrain sources and sinks in the East Asia region. After removing local influences, the time series CO_2 record was fitted to extract the seasonal cycle and long-term trend. The seasonal cycle, represented by the peak-to-peak amplitude, was analyzed for the interannual variation pattern. The CO_2 amplitudes obtained showed a typical magnitude in the mid-latitudes of approximately 19.7 ppm, with the seasonal maximum appeared around the beginning of April and minimum around the beginning of August. We found that interannual variations in atmospheric CO_2 at the outflow region of the Asian continent were affected by the temperature in East Asia through strengthened effects on the seasonal maximum with a time lag of 1–2 years. It was likely that the terrestrial ecosystem in East Asia received this climatic signal and transmitted it to the atmospheric CO_2 amplitude. Interannual variations in ^{222}Rn indicated that circulation changes were also likely contributing to the decreasing amplitude since 2009. The observed growth rate was related to large-scale circulations such as the Southern Oscillation Index and the North Pacific Index.

The Supplement related to this article is available online at doi:10.5194/esdd-5-809-2014-supplement.

Acknowledgements. We thank H. Tanimoto, of the National Institute of Environmental Studies, H. Matsueda, of the Geochemical Laboratory, Meteorological Research Institute, and T. Irino, of Hokkaido University, for their help in observation. HYI is partially supported by the Grant-in-Aid for Scientific Research of the Ministry of Education, Culture, Sports, Science and Technology of Japan (MEXT, #23241002), and the GRENE Arctic Climate Change Research Project of MEXT.

ESDD
5, 809–848, 2014

References

Akimoto, H.: Global air quality and pollution, Science, 302, 1716–1719, 2003.

Barford, C. C., Wofsy, S. C., Goulden, M. L., Munger, J. W., Hammond, P. E., Urbanski, S. P., Hutyra, L., Saleska, S. R., Fitzjarrald, D., and Moore, K.: Factors controlling long- and short-term sequestration of atmospheric CO_2 in a mid-latitude forest, Science, 294, 1688–1691, 2001.

Boden, T. A., Marland, G., and Andres, R. J.: Global, Regional, and National Fossil-Fuel CO_2 Emissions, Carbon Dioxide Information Analysis Center, Oak Ridge National Laboratory, US Department of Energy, Oak Ridge, Tenn., USA, 10.3334/CDIAC/00001_V2013, 2013.

Bond-Lamberty, B. and Thomson, A. M.: Temperature-associated increases in the global soil respiration record, Nature, 464, 579–582, 2010.

Braswell, B. H., Schimel, D. S., Linder, E., and Moore III, B.: The response of global terrestrial ecosystems to interannual temperature variability, Science, 278, 870–872, 1997.

Buermann, W., Lintner, B. R., Koven, C. D., Angert, A., Pinzon, J. E., Tucker, C. J., and Fung, I. Y.: The changing carbon cycle at Mauna Loa Observatory, P. Natl. Acad. Sci. USA, 104, 4249–4254, 2007.

Carouge, C., Bousquet, P., Peylin, P., Rayner, P. J., and Ciais, P.: What can we learn from European continuous atmospheric CO_2 measurements to quantify regional fluxes – Part 1: Potential of the 2001 network, Atmos. Chem. Phys., 10, 3107–3117, doi:10.5194/acp-10-3107-2010, 2010a.

Carouge, C., Rayner, P. J., Peylin, P., Bousquet, P., Chevallier, F., and Ciais, P.: What can we learn from European continuous atmospheric CO_2 measurements to quantify regional fluxes – Part 2: Sensitivity of flux accuracy to inverse setup, Atmos. Chem. Phys., 10, 3119–3129, doi:10.5194/acp-10-3119-2010, 2010b.

Chen, X. Q., Hu, B., and Yu, R.: Spatial and temporal variation of phonological growing season and climate change impacts in temperate eastern China, Global Change Biol., 11, 1118–1130, 2005.

Ciais, P., Canadell, J. G., Luyssaert, S., Chevallier, F., Shvidenko, A., Poussi, Z., Jonas, M., Peylin, P., King, A. W., Schulze, E.-D., Piao, S., Rödenbeck, C., Peters, W., and Bréon, F.-M.: Can we reconcile atmospheric estimates of the Northern terrestrial carbon sink with land-based accounting?, Curr. Opin. Environ. Sust., 2, 1–6, 2010.

ESDD
5, 809–848, 2014

Ciais, P., Sabine, C., Bala, G., Bopp, L., Brovkin, V., Canadell, J., Chhabra, A., DeFries, R., Galloway, J., Heimann, M., Jones, C., Le Quéré, C., Myneni, R. B., Piao, S., and Thornton, P.: Carbon and Other Biogeochemical Cycles, in: Climate Change 2013: The Physical Science Basis, Contribution of Working Group I to the Fifth Assessment Report of the Intergovernmental Panel on Climate Change, edited by: Stocker, T. F., Qin, D., Plattner, G.-K., Tignor, M., Allen, S. K., Boschung, J., Nauels, A., Xia, Y., Bex, V., and Midgley, P. M., Cambridge University Press, Cambridge, UK and New York, NY, USA, 2013.

Cong, N., Wang, T., Nan, H., Ma, Y., Wang, X., Myneni, R. B., and Piao, S.: Changes in satellite-derived spring vegetation green-up date and its linkage to climate in China from 1982 to 2010: a multimethod analysis, Global Change Biol., 19, 881–891, doi:10.1111/gcb.12077, 2012.

Conway, T. J., Tans, P. P., Waterman, L. S., Thoning, K. W., Kitzis, D. R., Masarie, K. A., and Zhang, N.: Evidence for interannual variability of the carbon cycle from the National Oceanic and Atmospheric Administration/Climate Monitoring and Diagnostics Laboratory global air sampling network, J. Geophys. Res., 99, 22831–22855, 1994.

Czeplak, G. and Junge, C.: Studies of interhemispheric exchange in the troposphere by a diffusion model, Adv. Geophys., 18, 57–72, 1974.

DOE US: Carbon cycling and biosequestration: integrating biology and climate through systems science: report from the March 2008 workshop, DOE/SC-108, US Department of Energy Office of Science, available at: http://genomicscience.energy.gov/carboncycle/report/ (last access: 26 June 2014), 2008.

Fang, S. X., Zhou, L. X., Tans, P. P., Ciais, P., Steinbacher, M., Xu, L., and Luan, T.: In situ measurement of atmospheric CO_2 at the four WMO/GAW stations in China, Atmos. Chem. Phys., 14, 2541–2554, doi:10.5194/acp-14-2541-2014, 2014.

Francey, R. J., Trudinger, C. M., Van Der Schoot, M., Krummel, P. B., Steele, L. P., and Langenfelds, R. L.: Differences between trends in atmospheric CO_2 and the reported trends in anthropogenic CO_2 emissions, Tellus B, 62, 316–328, doi:10.1111/j.1600-0889.2010.00472.x, 2010.

Graven, H. D., Keeling, R. F., Piper, S. C., Patra, P. K., Stephens, B. B., Wofsy, S. C., Welp, L. R., Sweeney, C., Tans, P. P., Kelley, J. J., Daube, B. C., Kort, E. A., Santoni, G. W., and Bent, J. D.: Enhanced seasonal exchange of CO_2 by northern ecosystems since 1960, Science, 341, 1085–1089, 2013.

ESDD
5, 809–848, 2014

Haszpra, L., Barcza, Z., Hidy, D., Szilágyi, I., Dlugokencky, E., and Tans, P.: Trends and temporal variations of major greenhouse gases at a rural site in Central Europe, Atmos. Environ., 42, 8707–8716, doi:10.1016/j.atmosenv.2008.09.012, 2008.

Higuchi, K., Murayama, S., and Taguchi, S.: Quasi-decadal variation of the atmospheric CO_2 seasonal cycle due to atmospheric circulation changes: 1979–1998, Geophys. Res. Lett., 29, 1173, doi:10.1029/2001GL013751, 2002.

Hui, D., Luo, Y., and Katul, G.: Parititioning interannual variability in net ecosystem exchange between climatic variability and functional change, Tree Physiol., 23, 433–442, 2003.

Hurrell, J.: National Center for Atmospheric Research, The Climate Data Guide: North Pacific (NP) Index by Trenberth and Hurrell; monthly and winter, last modified 20 November 2013, available at: https://climatedataguide.ucar.edu/climate-data/north-pacific-np-index-trenberth-and-hurrell-monthly-and-winter (last access: 18 March 2014), 2013.

Inoue, H. Y. and Matsueda, H.: Measurements of atmospheric CO_2 from a meteorological tower in Tsukuba, Japan, Tellus B, 53, 205–219, 2001.

Inoue, H. Y., Fukazawa, Y., Tanimoto, H., Matsueda, H., Sawa, Y., and Wada, A.: Atmospheric CO_2 and O_3 observed on Rishiri Island from December 2006 to March 2007, Pap. Meteorol. Geophys., 59, 31–38, 2008.

Ito, A.: Decadal variability in the terrestrial carbon budget caused by the Pacific Decadal Oscillation and Atlantic Multidecadal Oscillation, J. Meteorol. Soc. Jpn., 89, 441–454, 2011.

Janssens, I. A., Lankreijer, H., Matteucci, G., Kowalski, A. S., Buchmann, N., Epron, D., Pilegaard, K., Kutsch, W., Longdoz, B., Grünwald, T., Montagnani, L., Dore, S., Rebmann, C., Moors, E. J., Grelle, A., Rannik, Ü., Morgenstern, K., Oltchev, S., Clement, R., Guðmundsson, J., Minerbi, S., Berbigier, P., Ibrom, A., Moncrieff, J., Aubinet, M., Bernhofer, C., Jensen, N. O., Vesala, T., Granier, A., Schulze, E.-D., Lindroth, A., Dolman, A. J., Jarvis, P. G., Ceulemans, R., and Valentini, R.: Productivity overshadows temperature in determining soil and ecosystem respiration across European forests, Global Change Biol., 7, 269–278, doi:10.1046/j.1365-2486.2001.00412.x, 2001.

Jeong, S. J., Ho, C. H., Gim, H. J., and Brown, M. E.: Phenology shifts at start vs. end of growing season in temperate vegetation over the Northern Hemisphere for the period 1982–2008, Global Change Biol., 17, 2385–2399, 2011.

Jones, P. D. and Moberg, A.: Hemispheric and large-scale surface air temperature variations: an extensive revision and an update to 2001, J. Climate, 16, 206–223, 2003.

ESDD
5, 809–848, 2014

Keeling, C. D.: The concentration and isotopic abundances of carbon dioxide in the atmosphere, Tellus, 12, 200–203, 1960.
Keeling, C. D., Bacastow, R. B., Carter, A. F., Piper, S. C., Whorf, T. P., Heimann, M., Mook, W. G., and Roeloffzen, H.: A three-dimensional model of atmospheric CO_2 transport based on observed winds: 1. Analysis of observational data, in: Aspects of Climate Variability in the Pacific and the Western Americas, edited by: Peterson, D. H., Geophys. Monogr. Ser., 55, 165–235, 1989.
Keeling, C. D., Chin, J. F. S., and Whorf, T. P.: Increased activity of northern vegetation inferred from atmospheric CO_2 measurements, Nature, 382, 146–148, 1996.
Keeling, C. D., Piper, S. C., Whorf, T. P., and Keeling, R. F.: Evolution of natural and anthropogenic fluxes of atmospheric CO_2 from 1957 to 2003, Tellus B, 63, 1–22, 2011.
Kimoto, M.: Simulated change of the east Asian circulation under global warming scenario, Geophys. Res. Lett., 32, L16701, doi:10.1029/2005GL023383, 2005.
Komhyr, W. D., Gammon, R. H., Harris, T. B., Waterman, L. S., Conway, T. J., Taylor, W. R., and Thoning, K. W.: Global atmospheric CO_2 distribution and variations from 1968–1982 NOAA/GMCC CO_2 flask sample data, J. Geophys. Res., 90, 5567–5596, 1985.
Lee, K., Wanninkhof, R., Takahashi, T., Doney, S. C., and Feely, R. A.: Low interannual variability in recent oceanic uptake of atmospheric carbon dioxide, Nature, 396, 155–159, 1998.
Lefsky, M. A.: A global forest canopy height map from the Moderate Resolution Imaging Spectroradiometer and the Geoscience Laser Altimeter System, Geophys. Res. Lett., 37, L15401, doi:10.1029/2010GL043622, 2010.
Levin, I., Graul, R., and Trivett, N. B. A.: Long-term observations of atmospheric CO_2 and carbon isotopes at continental sites in Germany, Tellus B, 47, 23–34, 1995.
Lintner, B. R., Buermann, W., Koven, C. D., and Fung, I. Y.: Seasonal circulation and Mauna Loa CO_2 variability, J. Geophys. Res., 111, D13104, doi:10.1029/2005JD006535, 2006.
Mahecha, M. D., Reichstein, M., Carvalhais, N., Lasslop, G., Lange, H., Seneviratne, S. I., Vargas, R., Ammann, C., Arain, M. A., Cescatti, A., Janssens, I. A., Migliavacca, M., Montagnani, L., and Richardson, A. D.: Global convergence in the temperature sensitivity of respiration at ecosystem level, Science, 329, 838–840, doi:10.1126/science.1189587, 2010.
Maksyutov, S., Takagi, H., Valsala, V. K., Saito, M., Oda, T., Saeki, T., Belikov, D. A., Saito, R., Ito, A., Yoshida, Y., Morino, I., Uchino, O., Andres, R. J., and Yokota, T.: Regional CO_2 flux estimates for 2009–2010 based on GOSAT and ground-based CO_2 observations, Atmos. Chem. Phys., 13, 9351–9373, doi:10.5194/acp-13-9351-2013, 2013.

ESDD
5, 809–848, 2014

Minejima, C., Kubo, M., Tohjima, Y., Yamagishi, H., Koyama, Y., Maksyutov, S., Kita, K., and Mukai, H.: Analysis of $\Delta O_2/\Delta CO_2$ ratios for the pollution events observed at Hateruma Island, Japan, Atmos. Chem. Phys., 12, 2713–2723, doi:10.5194/acp-12-2713-2012, 2012.

Monson, R. K., Lipson, D. L., Burns, S. P., Turnipseed, A. A., Delany, A. C., Williams, M. W., and Schmidt, S. K.: Winter forest soil respiration controlled by climate and microbial community composition, Nature, 439, 711–714, 2006.

Murayama, S., Saigusa, N., Chan, D., Yamamoto, S., Kondo, H., and Eguchi, Y.: Temporal variations of atmospheric CO_2 concentration in a temperate deciduous forest in central Japan, Tellus B, 55, 232–243, doi:10.1034/j.1600-0889.2003.00061.x, 2003.

Murayama, S., Higuchi, K., and Taguchi, S.: Influence of atmospheric transport on the interannual variation of the CO_2 seasonal cycle downward zero-crossing, Geophys. Res. Lett., 34, L04811, doi:10.1029/2006GL028389, 2007.

Myhre, G., Shindell, D., Bréon, F.-M., Collins, W., Fuglestvedt, J., Huang, J., Koch, D., Lamarque, J.-F., Lee, D., Mendoza, B., Nakajima, T., Robock, A., Stephens, G., Takemura, T., and Zhang, H.: Anthropogenic and Natural Radiative Forcing, in: Climate Change 2013: The Physical Science Basis, Contribution of Working Group I to the Fifth Assessment Report of the Intergovernmental Panel on Climate Change, edited by: Stocker, T. F., Qin, D., Plattner, G.-K., Tignor, M., Allen, S. K., Boschung, J., Nauels, A., Xia, Y., Bex, V., and Midgley, P. M., Cambridge University Press, Cambridge, UK and New York, NY, USA, 2013.

Myneni, R. B., Dong, J., Tucker, C. J., Kaufmann, R. K., Kauppi, P. E., Liski, J., Zhou, L., Alexeyev, V., and Hughes, M. K.: A large carbon sink in the woody biomass of northern forests, P. Natl. Acad. Sci. USA, 98, 14784–14789, 2001.

Nisbet, E. and Weiss, R.: Top-down versus bottom-up, Science, 328, 1241, doi:doi:10.1126/science.1189936, 2010.

Nishina, K., Ito, A., Beerling, D. J., Cadule, P., Ciais, P., Clark, D. B., Falloon, P., Friend, A. D., Kahana, R., Kato, E., Keribin, R., Lucht, W., Lomas, M., Rademacher, T. T., Pavlick, R., Schaphoff, S., Vuichard, N., Warszawaski, L., and Yokohata, T.: Quantifying uncertainties in soil carbon responses to changes in global mean temperature and precipitation, Earth Syst. Dynam., 5, 197–209, doi:10.5194/esd-5-197-2014, 2014.

Niwa, Y., Patra, P. K., Sawa, Y., Machida, T., Matsueda, H., Belikov, D., Maki, T., Ikegami, M., Imasu, R., Maksyutov, S., Oda, T., Satoh, M., and Takigawa, M.: Three-dimensional variations of atmospheric CO_2: aircraft measurements and multi-transport model simulations, Atmos. Chem. Phys., 11, 13359–13375, doi:10.5194/acp-11-13359-2011, 2011.

ESDD
5, 809–848, 2014

Niwa, Y., Machida, T., Sawa, Y., Matsueda, H., Schuck, T. J., Brenninkmeijer, C. A. M., Imasu, R., and Satoh, M.: Imposing strong constraints on tropical terrestrial CO_2 fluxes using passenger aircraft based measurements, J. Geophys. Res., 117, D11303, doi:10.1029/2012JD017474, 2012.

Niwa, Y., Tsuboi, K., Matsueda, H., Sawa, Y., Machida, T., Nakamura, M., Kawasato, T., Saito, K., Takatsuji, S., Tsuji, K., Nishi, H., Dehara, K., Baba, Y., Kuboike, D., Iwatsubo, S., Ohmori, H., and Hanamiya, Y.: Seasonal variations of CO_2, CH_4, N_2O and CO in the mid-troposphere over the Western North Pacific observed using a C-130H Cargo Aircraft, J. Meteorol. Soc. Jpn., 92, 55–70, doi:10.2151/jmsj.2014-104, 2014.

NOAA Earth System Research Laboratory: The NOAA annual greenhouse gas index (AGGI), available at: http://www.esrl.noaa.gov/gmd/aggi/, last access: 18 March 2014.

Patra, P. K., Ishizawa, M., Maksyutov, S., Nakazawa, T., and Inoue, G.: Role of biomass burning and climate anomalies for land–atmosphere carbon fluxes based on inverse modeling of atmospheric CO_2, Global Biogeochem. Cy., 19, GB3005, doi:10.1029/2004GB002258, 2005.

Patra, P. K., Niwa, Y., Schuck, T. J., Brenninkmeijer, C. A. M., Machida, T., Matsueda, H., and Sawa, Y.: Carbon balance of South Asia constrained by passenger aircraft CO_2 measurements, Atmos. Chem. Phys., 11, 4163–4175, doi:10.5194/acp-11-4163-2011, 2011.

Peters, W., Jacobson, A. R., Sweeney, C., Andrews, A. E., Conway, T. J., Masarie, K., Miller, J. B., Bruhwiler, L. M. P., P'etron, G., Hirsch, A. I., Worthy, D. E. J., van der Werf, G. R., Randerson, J. T., Wennberg, P. O., Krol, M. C., and Tans, P. P.: An atmospheric perspective on North American carbon dioxide exchange: CarbonTracker, P. Natl. Acad. Sci. USA, 104, 18925–18930, 2007.

Peters, W., Krol, M. C., Van Der Werf, G. R., Houweling, S., Jones, C. D., Hughes, J., Schaefer, K., Masarie, K. A., Jacobson, A. R., Miller, J. B., Cho, C. H., Ramonet, M., Schmidt, M., Ciattaglia, L., Apadula, F., Heltai, D., Meinhardt, F., Di Sarra, A. G., Piacentino, S., Sferlazzo, D., Aalto, T., Hatakka, J., Ström, J., Haszpra, L., Meijer, H. A. J., Van Der Laan, S., Neubert, R. E. M., Jordan, A., Rodó, X., Morguí, J.-A., Vermeulen, A. T., Popa, E., Rozanski, K., Zimnoch, M., Manning, A. C., Leuenberger, M., Uglietti, C., Dolman, A. J., Ciais, P., Heimann, M., and Tans, P. P.: Seven years of recent European net terrestrial carbon dioxide exchange constrained by atmospheric observations, Global Change Biol., 16, 1317–1337, doi:10.1111/j.1365-2486.2009.02078.x, 2010.

Peterson, T. C. and Russell, S. V.: An overview of the Global Historical Climatology Network temperature database, B. Am. Meteorol. Soc., 78, 2837–2849, 1997.

ESDD
5, 809–848, 2014

Peylin, P., Law, R. M., Gurney, K. R., Chevallier, F., Jacobson, A. R., Maki, T., Niwa, Y., Patra, P. K., Peters, W., Rayner, P. J., Rödenbeck, C., van der Laan-Luijkx, I. T., and Zhang, X.: Global atmospheric carbon budget: results from an ensemble of atmospheric CO_2 inversions, Biogeosciences, 10, 6699–6720, doi:10.5194/bg-10-6699-2013, 2013.

Piao, S., Friedlingstein, P., Ciais, P., Viovy, N., and Demarty, J.: Growing season extension and its effects on terrestrial carbon flux over the last two decades, Global Biogeochem. Cy., 21, GB3018, doi:10.1029/2006GB002888, 2007.

Piao, S., Wang, X., Ciais, P., Zhu, B., Wang, T., and Liu, J.: Changes in satellite-derived vegetation growth trend in temperate and boreal Eurasia from 1982 to 2006, Global Change Biol., 17, 3228–3239, doi:10.1111/j.1365-2486.2011.02419.x, 2011.

Prytherch, J., Yelland, M. J., Pascal, R. W., Moat, B. I., Skjelvan, I., and Neill, C. C.: Direct measurements of the CO_2 flux over the ocean: development of a novel method, Geophys. Res. Lett., 37, L03607, doi:10.1029/2009GL041482, 2010.

Ramonet, M., Ciais, P., Aalto, T., Aulagnier, C., Chevallier, F., Cipriano, D., Conway, T. J., Haszpra, L., Kazan, V., Meinhardt, F., Paris, J.-D., Schmidt, M., Simmonds, P., Xueref-Rémy, I., and Necki, J. N.: A recent build-up of atmospheric CO_2 over Europe, Part 1: Observed signals and possible explanations, Tellus B, 62, 1–13, 2010.

Richardson, A. D., Black, T. A., Ciais, P., Delbart, N., Friedl, M. A., Gobron, N., Hollinger, D. Y., Kutsch, W. L., Longdoz, B., Luyssaert, S., Migliavacca, M., Montagnani, L., Munger, J. W., Moors, E., Piao, S. L., Rebmann, C., Reichstein, M., Saigusa, N., Tomelleri, E., Vargas, R., and Varlagin, A.: Influence of spring and autumn phonological transitions on forest ecosystem productivity, Philos. T. Roy. Soc. B, 365, 3227–3246, 2010.

Rödenbeck, C., Gerbig, C., Trusilova, K., and Heimann, M.: A two-step scheme for high-resolution regional atmospheric trace gas inversions based on independent models, Atmos. Chem. Phys., 9, 5331–5342, doi:10.5194/acp-9-5331-2009, 2009.

Saha, S., Moorthi, S., Pan, H.-L., Wu, X., Wang, J., Nadiga, S., Tripp, P., Kistler, R., Woollen, J., and Behringer, D.: The NCEP climate forecast system reanalysis, B. Am. Meteorol. Soc., 91, 1015–1057, doi:10.1175/2010BAMS3001.1, 2010.

Saigusa, N., Ichii, K., Murakami, H., Hirata, R., Asanuma, J., Den, H., Han, S.-J., Ide, R., Li, S.-G., Ohta, T., Sasai, T., Wang, S.-Q., and Yu, G.-R.: Impact of meteorological anomalies in the 2003 summer on Gross Primary Productivity in East Asia, Biogeosciences, 7, 641–655, doi:10.5194/bg-7-641-2010, 2010.

ESDD
5, 809–848, 2014

Séférian, R., Bopp, L., Swingedouw, D., and Servonnat, J.: Dynamical and biogeochemical control on the decadal variability of ocean carbon fluxes, Earth Syst. Dynam., 4, 109–127, doi:10.5194/esd-4-109-2013, 2013.

Teklemariam, T. A., Lafleur, P. M., Moore, T. R., Roulet, N. T., and Humphreys, E. R.: The direct and indirect effects of inter-annual meteorological variability on ecosystem carbon dioxide exchange at a temperate ombrotrophic bog, Agr. Forest Meteorol., 150, 1402–1411, 2010.

Tans, P. and Keeling, R.: NOAA/ESRL site, available at: http://www.esrl.noaa.gov/gmd/ccgg/trends/, last access: 3 April 2014.

Thoning, K. W., Tans, P. P., and Komhyr, W. D.: Atmospheric carbon dioxide at Mauna Loa Observatory: 2. Analysis of the NOAA/GMCC data, 1974–1985, J. Geophys. Res., 94, 8549–8565, 1989.

Wang, X., Piao, S., Ciais, P., Friedlingstein, P., Myneni, R. B., Cox, P., Heimann, M., Miller, J., Peng, S., Wang, T., Yang, H., and Chen, A.: A two-fold increase of carbon cycle sensitivity to tropical temperature variations, Nature, 506, 212–215, doi:10.1038/nature12915, 2014.

Wayne Polley, H., Frank, A. B., Sanabria, J., and Phillips, R. L.: Interannual variability in carbon dioxide fluxes and flux–climate relationships on grazed and ungrazed northern mixed-grass prairie, Global Change Biol., 14, 1620–1632, doi:10.1111/j.1365-2486.2008.01599.x, 2008.

WMO: Executive Council, forty-fourth session, Geneva, 22 June–4 July 1992: abridged report with resolutions, World Meteorological Organization, Geneva, Switzerland, 1992.

WMO: World Meteorological Organization – World Data Centre for Greenhouse Gases (WDCGG) Data Summary: Greenhouse Gases and Other Atmospheric Gases, No. 37, Japan Meteorological Agency, available at: http://ds.data.jma.go.jp/gmd/wdcgg/pub/products/summary/sum37/sum37.pdf (last access: 18 March 2014), 2013.

Wu, X. and Liu, H.: Consistent shifts in spring vegetation green-up date across temperate biomes in China, 1982–2006, Global Change Biol., 19, 870–880, doi:10.1111/gcb.12086, 2012.

Wunch, D., Wennberg, P. O., Messerschmidt, J., Parazoo, N. C., Toon, G. C., Deutscher, N. M., Keppel-Aleks, G., Roehl, C. M., Randerson, J. T., Warneke, T., and Notholt, J.: The covariation of Northern Hemisphere summertime CO_2 with surface temperature in boreal regions, Atmos. Chem. Phys., 13, 9447–9459, doi:10.5194/acp-13-9447-2013, 2013.

ESDD
5, 809–848, 2014

Yu, G. R., Zhu, X. J., Fu, Y. L., He, H. L., Wang, Q. F., Wen, X. F., Li, X. R., Zhang, L. M., Zhang, L., Su, W., Li, S. G., Sun, X. M., Zhang, Y. P., Zhang, J. H., Yan, J. H., Wang, H. M., Zhou, G. S., Jia, B. R., Xiang, W. H., Li, Y. N., Zhao, L., Wang, Y. F., Shi, P. L., Chen, S. P., Xin, X. P., Zhao, F. H., Wang, Y. Y., and Tong, C. L.: Spatial patterns and climate drivers of carbon fluxes in terrestrial ecosystems of China, Global Change Biol., 19, 798–810, doi:10.1111/gcb.12079, 2012.

Zeng, N., Yoon, J. H., Vintzileos, A., Collatz, G. J., Kalnay, E., Mariotti, A., Kumar, A., Busalacchi, A., and Lord, S.: Dynamical prediction of terrestrial ecosystems and the global carbon cycle: a 25-year hindcast experiment, Global Biogeochem. Cy., 22, GB4015, doi:10.1029/2008GB003183, 2008.

Zhang, X., Gurney, K. R., Peylin, P., Chevallier, F., Law, R. M., Patra, P. K., Rayner, P. J., Röedenbeck, C., and Krol, M.: On the variation of regional CO_2 exchange over temperate and boreal North America, Global Biogeochem. Cy., 27, 991–1000, 2013.

Zhou, L., Tang, J., Wen, Y., Li, J., Yan, P., and Zhang, X.: The impact of local winds and long-range transport on the continuous carbon dioxide record at Mount Waliguan, China, Tellus B, 55, 145–158, doi:10.1034/j.1600-0889.2003.00064.x, 2003.

Zhu, C., Inoue, Y. H., Matsueda, H., Sawa, Y., Niwa, Y., Wada, A., and Tanimoto, H.: Influence of Asian outflow on Rishiri Island, northernmost Japan: application of radon as a tracer for characterizing fetch regions and evaluating a global 3D model, Atmos. Environ., 50, 174–181, doi:10.1016/j.atmosenv.2011.12.043, 2012.

Zhu, C., Nakayama, M., and Inoue, Y. H.: Continuous measurement of CO_2 flux through the snowpack in a dwarf bamboo ecosystem on Rishiri Island, Hokkaido, Japan, Polar Science, doi:10.1016/j.polar.2014.04.003, in press, 2014.

ESDD
5, 809–848, 2014

Table 1. Linear correlation coefficients (R^2) between amplitude anomalies at Rishiri Island and one-year lagged anomalies of temperature and precipitation in East Asia (EA), broad East Asia (BEA), the Northern Hemisphere (NH) and the globe (GL) in 2006–2013[a].

	with temperature				with precipitation			
Period[b]	EA	BEA	NH	GL	EA	BEA	NH	GL
Previous year[c]	0.28	0.18	−0.18	−0.17	−0.20	0.02	−0.10	−0.01
Apr–Mar	0.73**	0.73**	0.03	−0.04	0.00	−0.13	−0.20	−0.16
Aug–Mar	0.58*	0.62*	0.15	0.11	−0.10	−0.09	−0.20	−0.19
Oct–Mar	0.50*	0.57*	0.22	0.18	−0.05	0.21	−0.14	−0.11
Mar	0.53*	0.56*	0.36	0.39	0.37	0.06	0.18	−0.16
Sep–Aug	0.48	0.46	−0.19	−0.19	−0.17	0.11	−0.09	−0.09
Mar–Aug	0.36	0.20	0.03	0.08	−0.18	−0.12	−0.17	−0.10
Jun–Aug	−0.19	0.11	0.55*	0.72**	−0.17	−0.19	−0.18	−0.18
Aug	−0.20	−0.19	0.15	0.35	0.11	−0.11	−0.13	−0.14

[a] (1) *, $p < 0.05$; **, $p < 0.01$; (2) −, negative correlations.
[b] Except for "Previous year", temperature and precipitation anomalies are calculated for each of the periods counted in reverse from the month in the previous year (−1 year) to the month of one year prior (−2 year); see text for details.
[c] Correlations are amplitude anomalies with temperature and precipitation anomalies of the previous year (January to December).

ESDD
5, 809–848, 2014

Table 2. Linear correlation coefficients (R^2) between maximum (max ΔCO_2) and minimum ΔCO_2 (min ΔCO_2) anomalies at Rishiri Island and one-year lagged anomalies of temperature in East Asia (EA) and broad East Asia (BEA) in 2006–2013[a].

	EA		BEA	
Period	max ΔCO_2	min ΔCO_2	max ΔCO_2	min ΔCO_2
Apr–Mar	0.77^{**}	0.59^{*}	0.71^{*}	0.62^{*}
Aug–Mar	0.76^{**}	0.43^{*}	0.73^{**}	0.51^{*}
Oct–Mar	0.77^{**}	0.34	0.72^{**}	0.45^{*}
Mar	0.76^{**}	0.33	0.82^{**}	0.38

[a] *, $p < 0.05$; **, $p < 0.01$.
[b] Temperature anomalies are calculated in each of periods counted in reverse from the month in the previous year (−1 year) to the month of one year prior (−2 year); see text for details.

ESDD
5, 809–848, 2014

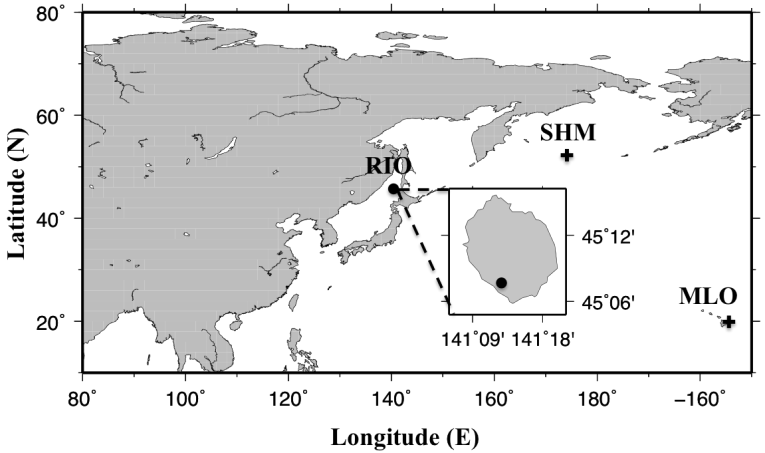

Figure 1. The location of Rishiri Island in East Asia and Rishiri Observatory (RIO, 45.10° N, 141.20° E) in the island (filled cycle). The Mauna Loa Observatory (MLO, 19.54° N, 155.58° W) and the Shemya Island (SHM, 52.72° N, 174.10° E) CO_2 observation sites mentioned in the study are also shown.

ESDD
5, 809–848, 2014

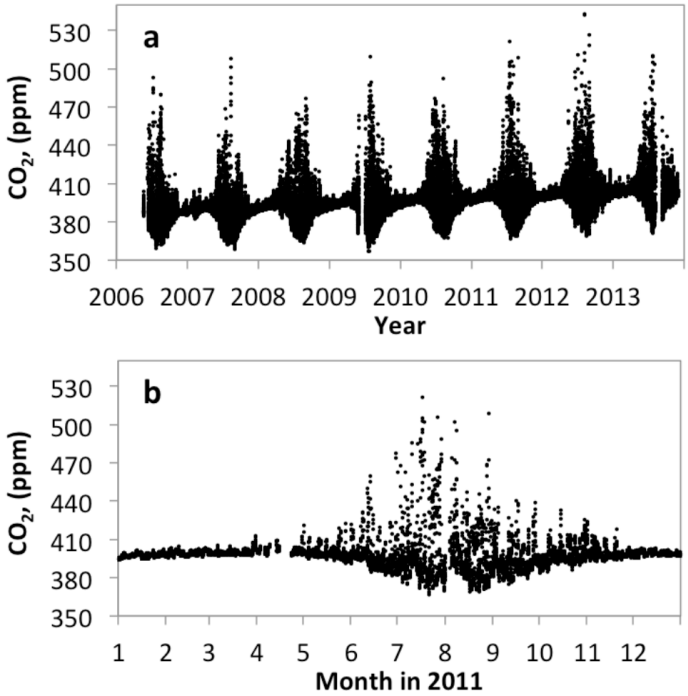

Figure 2. The original observed hourly CO_2 dataset: **(a)** the records from May 2006 to November 2013; **(b)** the records in 2011.

ESDD
5, 809–848, 2014

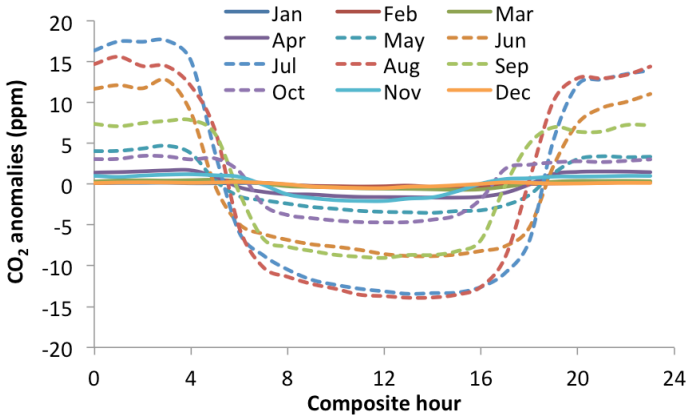

Figure 3. Diurnal variation of atmospheric CO_2 at Rishiri Island shown by the deviation in hourly values from the monthly means in 2006–2013.

ESDD
5, 809–848, 2014

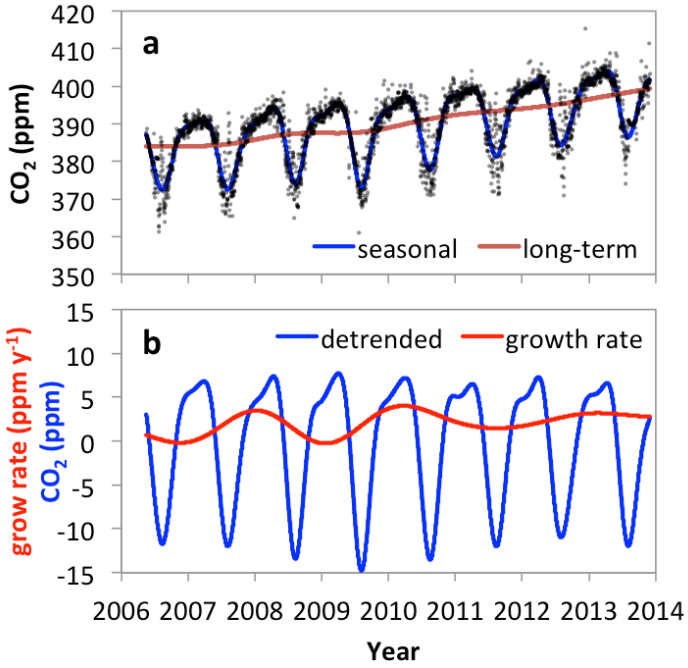

Figure 4. (a) The seasonal cycle and long-term trend along with daily means from observation (dotted); and **(b)** the de-trended cycle (ΔCO_2) along with the grow rate at Rishiri Island in 2006–2013.

ESDD
5, 809–848, 2014

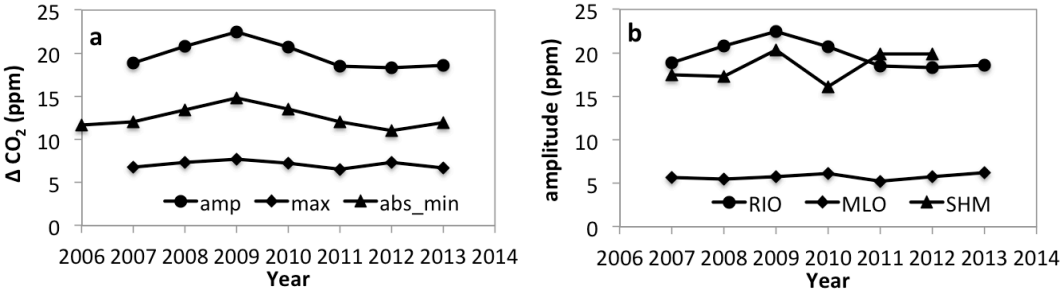

Figure 5. The interannual variations in seasonal amplitude: **(a)** the seasonal amplitude along with the maximum and absolute value of the minimum ΔCO_2 of the year; **(b)** the seasonal amplitude at RIO, in comparison with that in Shemya Island (SHM) and Mauna Loa (MLO) obtained from NOAA.

ESDD
5, 809–848, 2014

Temporal variations in atmospheric CO_2 on Rishiri Island in 2006–2013

C. Zhu and
H. Yoshikawa-Inoue

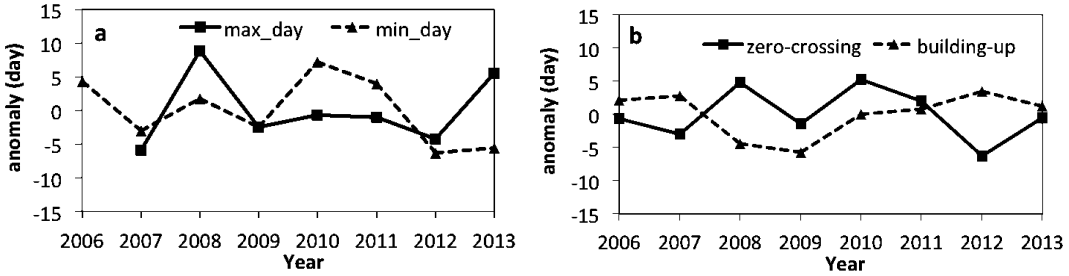

Figure 6. The interannual variations in seasonal phase: **(a)** the anomaly of maximum and minimum days with respect to the mean of 3 April for maximum and 8 August for minimum days; and **(b)** the anomaly of zero-crossing and buildup days with respect to the mean of 2 June for zero-crossing and 23 October for buildup days.

ESDD
5, 809–848, 2014

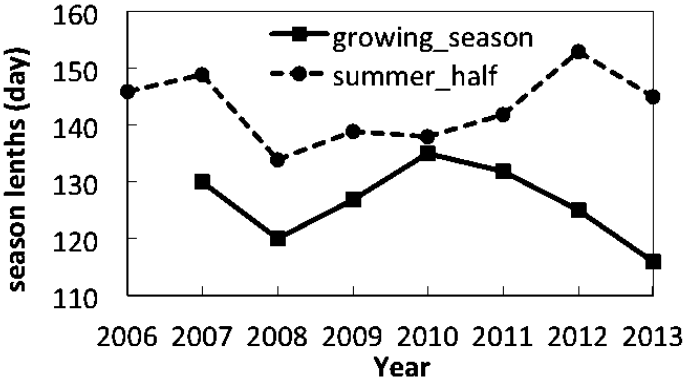

Figure 7. The interannual variations in growing season and summer half lengths.

ESDD
5, 809–848, 2014

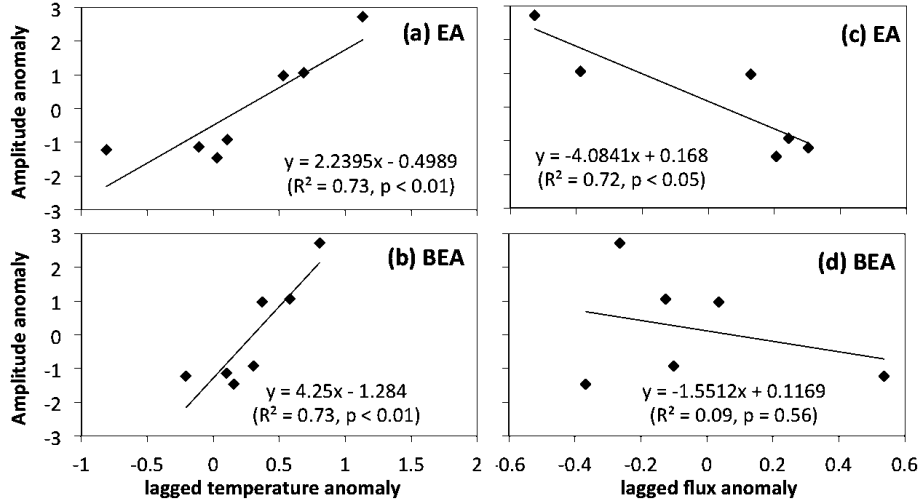

Figure 8. Relations of amplitude anomalies at Rishiri Island with the lagged temperature anomaly (means from March in the previous year to April in the year prior) in **(a)** East Asia and **(b)** broad East Asia, and with lagged flux anomalies (previous year) in **(c)** East Asia and **(d)** broad East Asia during 2006–2013.

ESDD
5, 809–848, 2014

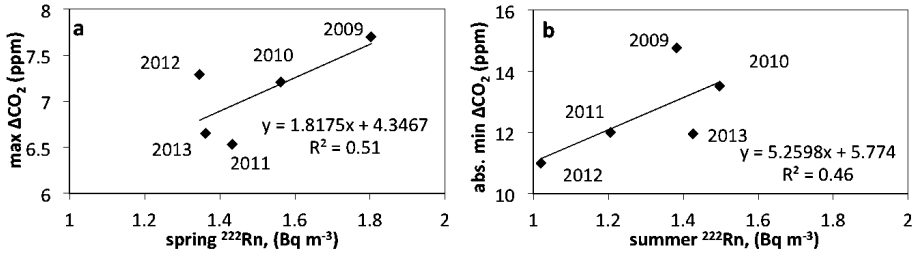

Figure 9. The linear relations between annual ΔCO_2 and ^{222}Rn concentration: **(a)** maximum ΔCO_2 and ^{222}Rn concentration in spring (March–May); and **(b)** absolute value of minimum ΔCO_2 and ^{222}Rn concentration in summer (June–August).

ESDD
5, 809–848, 2014

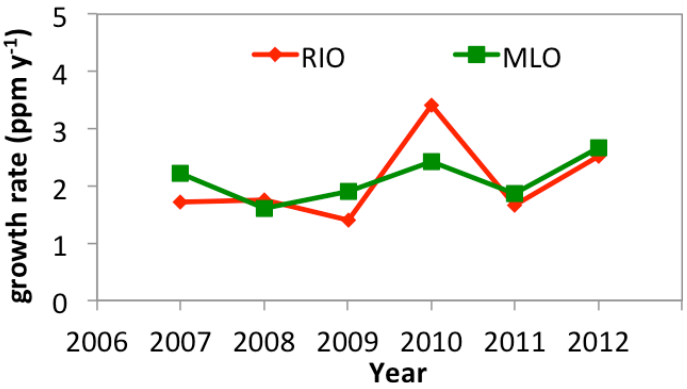

Figure 10. The interannual variations in growth rate at RIO. The growth rate at the MLO site is also shown for comparison.

ESDD
5, 809–848, 2014

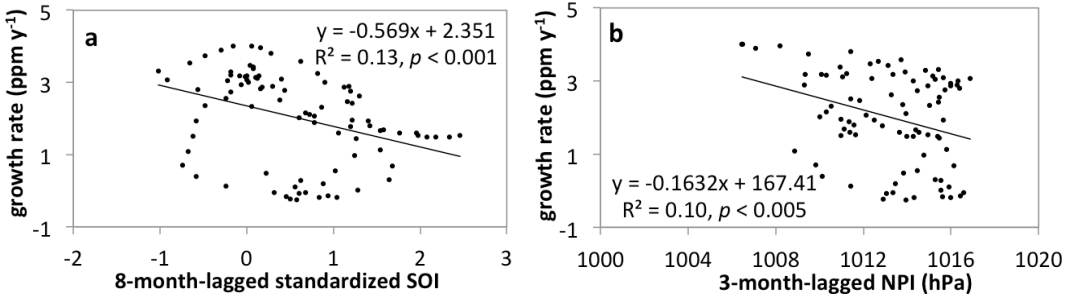

Figure 11. The lagged linear relations between the monthly growth rate at RIO and SOI and NPI: **(a)** the relation between growth rate with 8 month lagged standardized SOI; **(b)** the relation between growth rate with 3 month lagged NPI.

ESDD
5, 809–848, 2014